KFUPM
Journal of Undergraduate Research International

Diamond Open Access 119

Article Material Science and Engineering

Pt- and Pd-Based Carbon-Supported Catalysts for Efficient Hydrogen Storage via Toluene Hydrogenation in LOHC Systems

Ghala Al Hetelah and M. Nasiruzzaman Shaikh*

Cite https://doi.org/10.64589/juri/231556

Submitted: April 23, 2026 **Revised:** May 10, 2026 **Accepted:** May 15, 2026

ABSTRACT

This study examined the performance of platinum and palladium catalysts on activated carbon and sulfur-doped carbon supports for hydrogenating toluene and storing hydrogen in liquid organic hydrogen carrier systems. A wet impregnation method was used to synthesize the catalysts, which were systematically characterized using X-ray diffraction (XRD), scanning electron microscopy with energy-dispersive spectroscopy, and transmission electron microscopy. XRD analysis confirmed that the predominantly amorphous nature of the carbon supports the high dispersion of the metal species, whereas microscopic analysis showed clear morphological differences caused by sulfur doping and differences in the dispersion and crystallinity of the metal. The catalytic performance was tested in a high-pressure batch reactor with a temperature ranging between 100 and 200 °C and a pressure of hydrogen of up to 70 bar. Among the catalysts, 1% Pt/AC was found to be the most active catalyst, with a toluene conversion of 73.3% at 150 °C and 50 bar H_2, whereas the Pd-based and sulfur-doped catalysts were much less active. All catalysts showed good selectivity for methylcyclohexane (>99%). The parametric analyses showed that the heating temperature had a dominant influence in the catalytic performance, which was most effective at 150 °C, whereas an increase in hydrogen pressure yielded a moderate increase in conversion. The superior performance of 1% Pt/AC was attributed to the high metal dispersion and good metal–support interaction.

Keywords: hydrogen storage; LOHC; platinum; palladium; toluene

1. INTRODUCTION

Hydrogen is a promising clean energy carrier that has gained significant attention in both industrial and academic sectors because of its potential to meet the growing demands for transportation, electricity generation, and overall energy consumption, while reducing dependence on fossil fuels[1]. However, the low volumetric energy density of hydrogen renders its storage and transportation difficult, posing a major challenge to the realization of a hydrogen-based economy[2–4]. Therefore, the development of efficient technologies for hydrogen production, storage, and transportation is essential; however, hydrogen storage remains a critical challenge.

The traditional hydrogen storage methods, including high-pressure compression and cryogenic liquefaction, present considerable technical and economic obstacles that hinder their broad acceptance. Compression involves storage at pressures up to 700 bar, which not only demands high energy input but also poses severe safety issues because it requires strong and high-pressure container systems[5–8]. Liquefaction entails the cooling of hydrogen to very low temperatures (−253 °C), which poses significant problems in terms of energy requirements, infrastructure, and logistics of operation[3,5,7]. Neither of these methods is scalable or cost-efficient, which restricts their applicability to large-scale implementation. These shortcomings underscore the necessity of developing alternative hydrogen storage solutions to maximize the benefits of hydrogen as a clean energy carrier.

Liquid Organic Hydrogen Carriers (LOHCs) are receiving a lot of attention as a promising method of hydrogen storage and transportation. Many different LOHC systems have been studied, such as toluene/methylcyclohexane[9–12], benzene/cyclohexane[13–16], N-ethylcarbazole/dodecahydro-N-ethylcarbazole[17–20], dibenzyltoluene/perhydro-dibenzyltoluene[21–25], and benzyltoluene/perhydro-benzyltoluene[26–29]. The physicochemical properties and hydrogen storage ability of these hydrogen carrier pairs have shown a great potential. The toluene (TOL)/methylcyclohexane (MCH) system is considered one of the most promising LOHC systems available. This is in part because it has a relatively high hydrogen storage capability of 6.2 wt.%, high thermal stability and is compatible with the existing fuel distribution and transportation system[30]. Moreover, the use of TOL provides an attractive way of storing hydrogen at large scale, which is potentially cost-effective and practical, and is a promising option for future industrial application and suitable for a sustainable hydrogen economy[31].

Various studies have been conducted on the catalytic hydrogenation of toluene to methylcyclohexane (MCH), especially using noble metal catalysts such as Pt, Pd, Ru, and Rh[32–37]. Yang et al. synthesized mesoporous Pt/AC, Pt/Al_2O_3 and Pt/CeO_2 catalysts and studied their performance for hydrogenation of

Published under an exclusive license by KFUPM

TOL. Among these, Pt/CeO_2 displayed the best catalytic performance, 90.8% toluene conversion at 100 °C with a total selectivity towards MCH at 50 bar hydrogen pressure[38]. Similarly, Murata et al. investigated the influence of the particle size of Pt/Al_2O_3 catalysts and found that the activity of the catalysts increased with an increase in the particle size up to 2.5 nm, after which they did not find any further increase in the activity of the catalysts[32].

Although Pt-based catalytic systems have been studied in detail for the hydrogenation of toluene, the influence of various noble metals and heteroatom-doped carbon supports has not been clarified. In particular, the effects of the incorporation of sulfur on the dispersion of metals, structure of the supports, and catalytic activity for LOHC systems have not been studied systematically. Hence, this study aimed to understand the synergistic effects of the type of metal and sulfur-doped carbon supports in the hydrogenation reaction under practical reaction conditions.

In this study, toluene hydrogenation was conducted to investigate the catalyst performance in LOHC systems. Catalysts based on platinum and palladium on AC and sulfur-doped carbon were prepared and thoroughly studied. X-ray diffraction (XRD), scanning electron microscopy (SEM), transmission electron microscopy (TEM), and Raman spectroscopy were used to characterize the structure–property relationships comprehensively. The hydrogenation conditions were varied to determine the catalytic activity of these materials at temperatures in the 100–200 °C range at a hydrogen pressure of 50 bar.

2. MATERIALS AND METHODS

2.1. Materials. Chemicals and reagents were purchased from Sigma-Aldrich and used as received. The dry and deoxygenated solvents were prepared using standard procedures. Deionized water (DI) (specific conductivity: 18/2 MΩ) was used in all experiments.

2.2. Synthesis of Catalyst. A 1% Pt/AC catalyst was synthesized using a wet impregnation method, followed by chemical reduction and thermal post-treatment. First, 3.67 mg of $PtCl_2$ was dissolved in DI. The resulting solution was stirred at 20 °C for 5 min, and then ultrasonicated for 20 min to obtain a homogeneous Pt precursor solution. Subsequently, 496.33 mg of AC was gradually added to the precursor solution under continuous stirring. The mixture was stirred at room temperature for 4 h to ensure the proper impregnation of the platinum precursor onto the carbon support. Subsequently, $NaBH_4$ was added as a reducing agent, and the suspension was stirred to complete the reduction process, resulting in a Pt/AC wet mixture. The obtained material was dried for 12 h at 110 °C, followed by calcination at 400 °C for 4 h using a heating rate of 5 °C min^{-1}. The final product obtained was a 1 wt.% Pt/AC catalyst. The same procedure was used to prepare other catalysts. The overall synthesis procedure is presented in Figure 1.

2.3. Catalyst Characterization Techniques.

2.3.1. X-ray diffraction (XRD). The synthesized materials were examined by XRD with a Rigaku Ultima-IV diffractometer with Cu Kα radiation (λ = 1.5406 Å). Diffraction measurements were taken at V = 40 kV and I = 25 mA, and the diffraction patterns over a 2θ range were obtained in ambient conditions for 20°to 130°. The crystallite size was determined using the Scherrer equation, i.e., equation (1):

$$D = \frac{0.89\lambda}{\Delta \cos\theta}, \tag{1}$$

where D refers to the crystal size in Å, λ is the wavelength of the X-ray used, Δ denotes the full width at half maximum (FWHM) of the diffraction peak, and θ is the diffraction angle.

2.3.2. Scanning electron microscopy (SEM):. SEM was used for surface morphology and microstructural features of the samples. The samples were dispersed in ethanol before analysis, and the dispersed suspensions were applied to alumina stubs with single-sided alumina adhesive tape. Energy-dispersive X-ray spectroscopy (EDS) equipped with a Lyra 3 detector system (Tescan, Czech Republic) was used to analyze the elemental composition and spatial distribution of the constituent elements of the materials using SEM. Elemental mapping was carried out to assess the homogeneity of the element distribution in the sample surface.

2.3.3. Transmission electron microscopy (TEM):. The prepared materials were studied by TEM on a FEI Titan microscope equipped with a Gatan 4k ×4k UltraScan 400SP CCD camera and operated at 200 kV. High-resolution transmission electron microscopy (HRTEM) was performed in a FEI Titan microscope, a 300 kV aberration-corrected electron microscope for nanoscale imaging of lattice fringes and crystallographic features. The samples were homogenized in ethanol by ultrasonic dispersion for TEM analysis. A small droplet of the suspension was drop-cast on a carbon-coated copper grid and left to air dry at room temperature before imaging.

3. EXPERIMENTAL WORK

3.1. Experimental Apparatus. The stirred batch reactor (100 mL) shown in Figure 2 was used for hydrogenation reactions. The reactor is designed of stainless steel, with the maximum temperature of 300 °C and the maximum pressure of 15 MPa. The heating was provided by an external heater surrounding the reactor vessel to provide a uniform temperature throughout the reaction system. The heating unit could be heated to a maximum temperature of 760 °C, and an effective sealing was performed by a high-temperature O-ring. The homogeneous mixing was achieved by using an internally mounted blade-type impeller. The impeller was magnetically driven by a DC motor (Bodine Electric Company, S/N 6037QQIA0016) that had a maximum speed of 2500 rpm, and speeds of up to 2000 rpm could be achieved within the reactor. A water chiller was used to continuously cool the drive system to prevent its demagnetization at high temperatures, while maintaining magnetic coupling stability. Two K-type thermocouples (1.58 mm diameter) were installed for continuous monitoring to maintain accurate temperature control within the reaction system. Moreover, a pressure transducer was also installed in the reactor system to monitor the pressure in the system during the hydrogenation process.

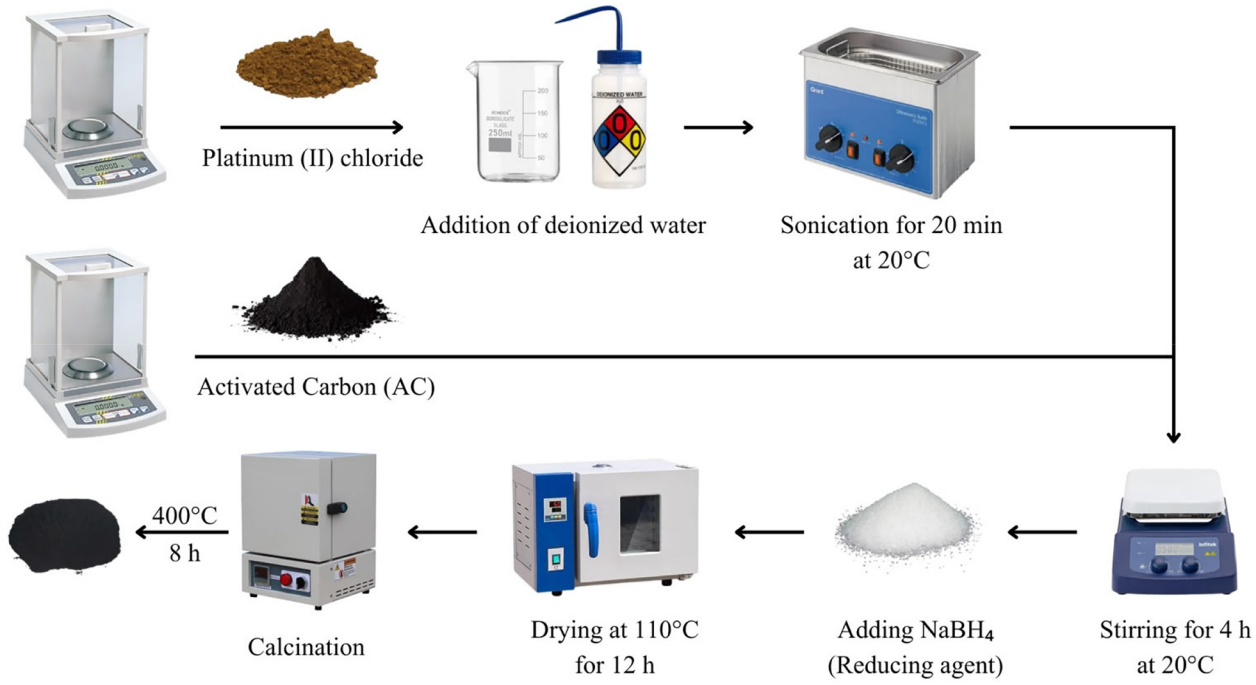


Figure 1. Schematic of the synthesis procedure for the Pt/AC catalyst

3.2. Experimental Procedure. Toluene (2 mL) and the catalyst (50 mg) were loaded into the reactor. The reactor was closed and then purged three times with hydrogen to remove the air. An automated control system was used to control the desired reaction temperature and stirring speed. After setting the operating conditions, hydrogen was fed into the reactor until the required pressure was reached and the heating system was switched on to start the reaction. At the end of the experiment the reactor was cooled, depressurized, and the reaction mixture was collected and filtered off. The liquid products were then analysed by gas chromatography–mass spectrometry (GC–MS) and the conversion of TOL calculated, as well as the identification of the products by their mass spectral signatures.

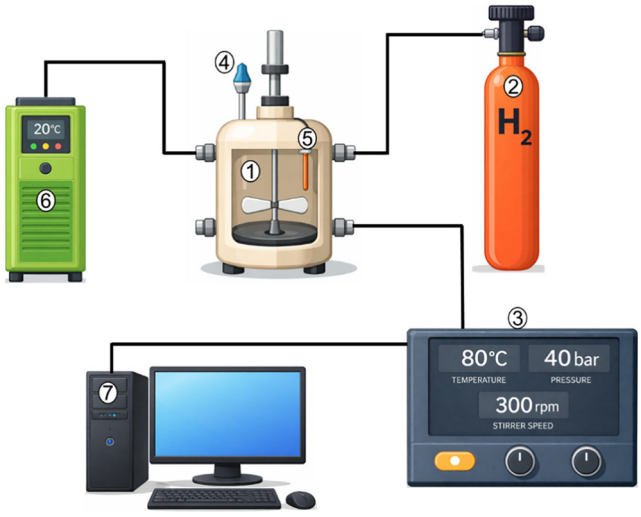


Figure 2. Schematic of the experimental setup (1. Autoclave, 2. hydrogen cylinder, 3. system controller, 4. pressure transducer, 5. K-type thermocouple, 6. water chiller, and 7. computer)

4. RESULTS AND DISCUSSION

4.1. XRD Characterization. Figure 3 shows the XRD patterns of the synthesized catalysts (1% Pt/AC, 1% Pd/AC, 1% Pt/S-C, and 1% Pd/S-C). A diffraction band with a central value of 20–30 is observed in all samples and was ascribed to the (002) plane of amorphous carbon, showing a largely disordered form of both the AC and sulfur-doped carbon supports. These samples lack sharp graphitic peaks, implying a low level of graphitization, which is a characteristic of carbonaceous materials. The slight broadening of the intensity of this diffraction feature in the sulfur-doped carbon-supported catalysts (1% Pt/S-C and 1% Pd/S-C) suggests that further incorporation of sulfur disrupts the carbon structure and increases structural disorder. This modification may influence electronic properties and metal–support interactions.

None of the catalysts show clear diffraction peaks indicative of the metallic Pt or Pd phases. This could be attributed to the low metal loading (1 wt.%) and the high dispersion of metal species on the carbon supports, resulting in crystallite sizes below the XRD detection limit. A weak and broad feature is observed at approximately 40°–45°degrees, which in the 1% Pd/AC case can be tentatively attributed to the (111) reflection of the face-centered cubic Pd, but its low intensity suggests the lack of crystallinity. The lack of Pt reflections further confirmed the presence of highly dispersed or amorphous Pt species. The XRD data indicate that the catalysts were mostly amorphous, with the diffraction patterns dominated by the carbon support. The large separation of Pt and Pd species deduced from the lack of typical metallic peaks is in line with the microscopic measurements and should prove advantageous for the catalytic hydrogenation of operations in LOHC systems.

4.2. Scanning Electron Microscopy (SEM). SEM and EDS were used to systematically analyze the morphology and

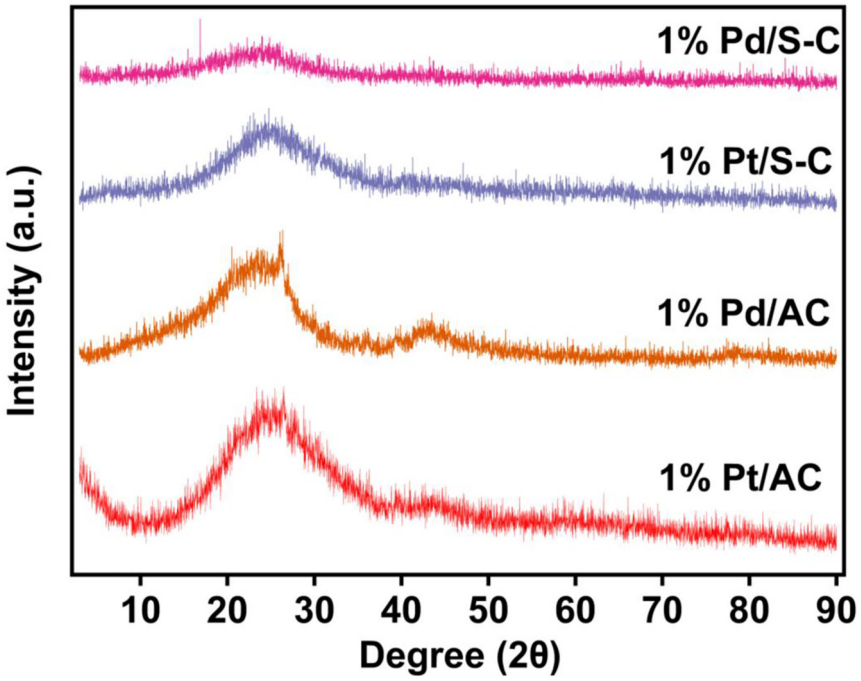


Figure 3. X-ray diffraction (XRD) patterns of 1% Pt/AC, 1% Pd/AC, 1% Pt/S-C, and 1% Pd/S-C catalysts

elemental composition of the synthesized catalysts, namely, 1% Pt/AC, 1% Pd/AC, 1% Pt/S-C, and 1% Pd/S-C. Figure 4 shows the corresponding SEM images, elemental mapping, and EDS spectra. The SEM micrographs indicate notable morphological differences between the catalysts supported on AC and those supported on sulfur-doped carbon. The 1% Pt/C catalyst (Figure 4a) has a heterogeneous and granular surface formed by irregularly shaped, agglomerated carbon particles, and it has a rather rough texture. The 1% Pd/C sample also shows a similar morphology (Figure 4b), indicating that metal deposition did not significantly alter the inherent structure of the AC support. By contrast, the carbon-supported catalysts with 1% Pt/S-C and 1% Pd/S-C (Figures 4c and 4d) have elongated, fibrous, and layered structures, suggesting that sulfur incorporation induces structural reorganization and increased anisotropy in the carbon matrix.

Elemental mapping (Figure 4) also supports the incorporation and uniform distribution of the constituent elements, including C, Pt (or Pd), O, and S, in the doped samples. The metal species are well-dispersed across the support without noticeable agglomeration, indicating good metal anchoring. In addition, the even distribution of sulfur in the doped catalysts confirms its successful incorporation into the carbon framework. EDS analysis confirms the metal loadings, with Pt and Pd contents of 1.0 wt.% and 0.9 wt.% in 1% Pt/C and 1% Pd/C, respectively, and slightly lower values of 0.4 wt.% Pt and 0.6 wt.% Pd in the sulfur-doped catalysts. Therefore, SEM–EDS analysis confirmed the successful deposition of Pt and Pd on both the activated and sulfur-doped carbon supports with good dispersion. Sulfur doping significantly alters carbon morphology, which may influence active site accessibility and catalytic performance. Elemental mapping verified the presence of C, Pt (or Pd), O, and S in the respective catalysts, with all elements being uniformly distributed and no evidence of significant metal agglomeration, confirming effective metal dispersion and sulfur incorporation.

4.3. Transmission Electron Microscopy (TEM). The morphology, microstructure, and crystallinity of the synthesized catalysts (1% Pt/AC, 1% Pd/AC, 1% Pt/S-C, and 1% Pd/S-C) were explained with the help of TEM, HRTEM, and selected area electron diffraction (SAED). Figure 5 shows the corresponding micrographs and diffraction patterns. The TEM images (Figure 5a–d) indicate strong morphological differences between the metal species and the support properties. The 1% Pt/AC catalyst (Figure 5a) has stacked, sheet-like carbon structures that have irregular overlapping layers, which correspond to aggregated graphitic domains. In comparison, the 1% Pd/AC (Figure 5b) shows a smaller and more disordered morphology, indicating the degree of dispersion in the porous structure of carbon. The 1% Pt/S-C catalyst (Figure 5c) exhibits relatively smooth and extended layered areas, indicating that the carbon structure was more confined and rearranged after incorporation of sulfur. The 1% Pd/S-C catalyst (Figure 5d) is composed of aggregated quasi-spherical nanoparticles with well-defined interfaces, which is a sign of localized particle growth and phase segregation.

Additional structural information was obtained from the HRTEM images (Figure 5a1–d1). The 1% Pt/AC and 1% Pd/AC catalysts (Figure 5a1 and 5b1) exhibit mostly diffuse contrast with poorly resolved lattice fringes, indicating highly dispersed metal species and low crystallinity or ultrafine particle sizes on the AC support. The same structural characteristics are found for 1% Pt/S-C (Figure 5c1), where no individual lattice fringes are observed, implying amorphous behavior or suggesting that the Pt is extremely small and highly dispersed. Conversely, the 1% Pd/S-C catalyst (Figure 5d1) exhibits clear lattice fringes, confirming the formation of crystalline Pd nanoparticles with a greater level of structural order. The SAED patterns (Figure 5a2–d2) further corroborate these observations. The 1% Pt/AC catalyst exhibits concentric rings of diffraction, which are typical of a polycrystalline structure with randomly oriented nanodomains.

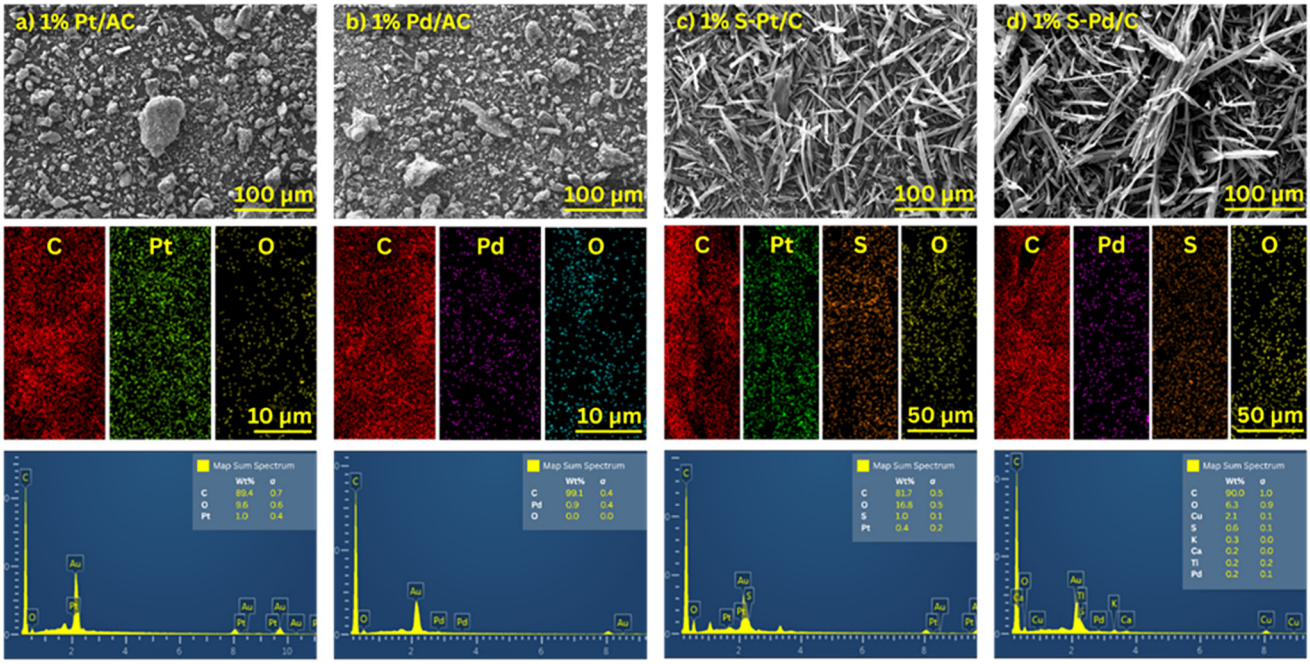


Figure 4. SEM images, elemental mapping, and EDS spectra of (a) 1% Pt/C, (b) 1% Pd/C, (c) 1% Pt/S-C, and (d) 1% Pd/S-C

Comparatively, the 1% Pd/AC and 1% Pt/S-C samples show broad and diffuse rings, which indicate the presence of mainly amorphous or poorly crystallized phases. The 1% Pd/S-C catalyst exhibits distinct diffraction spots overlaid on a faint diffuse background, indicating the presence of clear crystalline domains. Collectively, the TEM, HRTEM, and SAED analyses indicate that the composition and identity of the metals have a significant effect on the structural properties of the catalysts. The 1% Pd/S-C catalyst has the greatest level of crystallinity and most distinguishable nanoparticle formation, whereas the other catalysts exhibit highly dispersed and highly amorphous metal phases. Such structural variations are considered very important for regulating the catalytic behavior. The 1% Pd/S-C sample (Figure 5d2) consists of aggregated quasi-spherical nanoparticles with clearly distinguishable particle boundaries, indicating the formation of more localized crystalline domains.

4.4. Catalytic Evaluation for Hydrogenation of Toluene. The catalytic activities of the prepared catalysts (1% Pt/AC, 1% Pd/AC, 1% Pt/S-C, and 1% Pd/S-C) in the hydrogenation of toluene under the same reaction conditions (150 °C, 50 bar of H_2, 2 mL of toluene, and 50 mg catalyst) were compared. The catalytic activity strongly relies on the nature

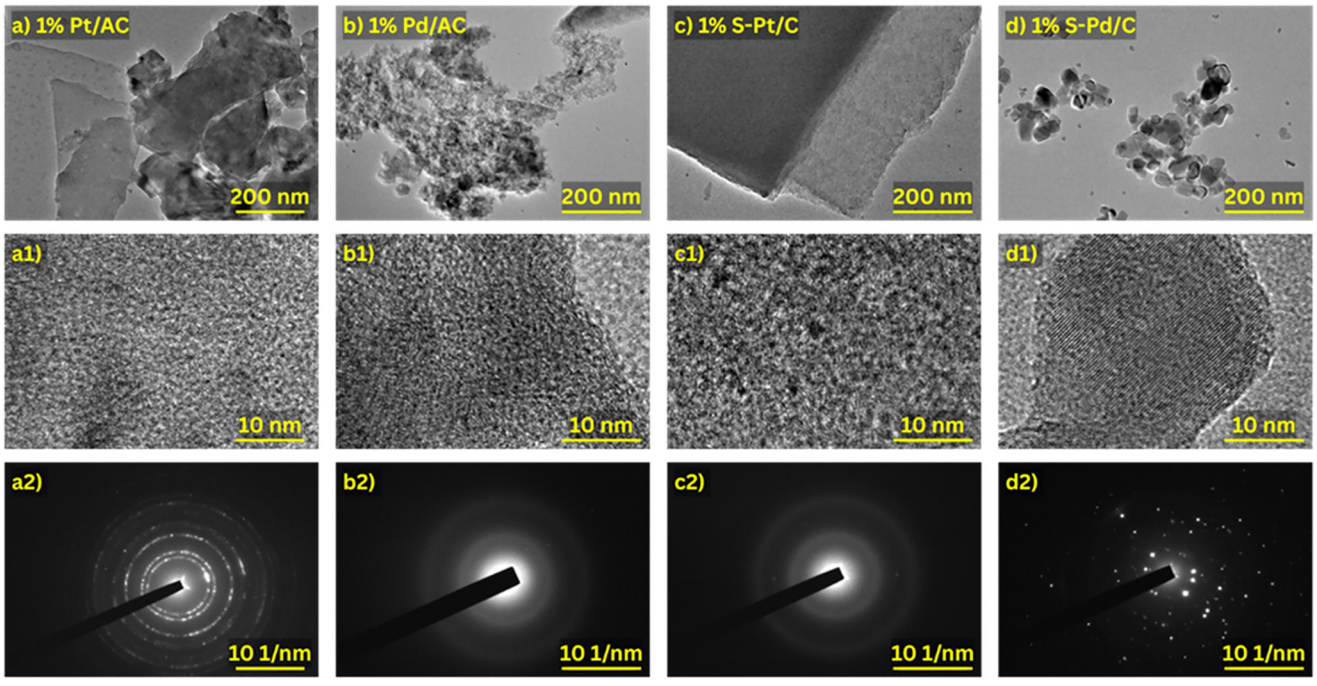


Figure 5. TEM, HRTEM, and SAED images of (a–a2) 1% Pt/AC, (b–b2) 1% Pd/AC, (c–c2) 1% Pt/S-C, and (d–d2) 1% Pd/S-C

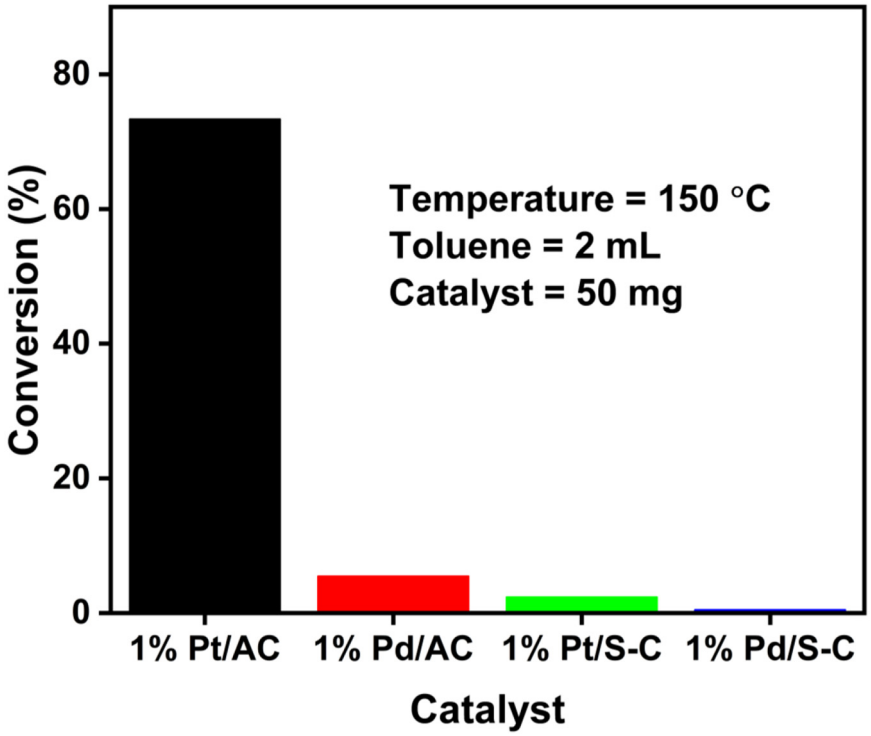


Figure 6. Toluene conversion over different catalysts (1 % Pt/AC, 1 % Pd/AC, 1 % Pt/S-C, and 1 % Pd/S-C) at 150 °C and 50 bar H2

of the active metal as well as the support. As shown in Figure 6, 1% Pt/AC is the most active material studied, with a toluene conversion of 73.3%. By comparison, 1% Pd/AC performs much worse, with a conversion of only 5.5%. The sulfur-doped catalysts are even less active, with only 2.4% and 0.5% conversion for 1% Pt/S-C and 1% Pd/S-C, respectively. All catalysts are highly selective towards MCH (>99%), indicating that the hydrogenation route was very selective regardless of the catalyst composition. The decreased activity of sulfur-doped carbon-supported catalysts is believed to result from the interactions between the metal and sulfur, which alter the electronic structure of the active sites and cause their partial blocking, thereby retarding hydrogen adsorption and activation[39,40]. Furthermore, sulfur doping may result in defects and/or modification of the carbon matrix, which can negatively affect metal dispersion and availability[41]. The lower activity of Pd-based catalysts is primarily due to differences in their hydrogenation behavior compared with that of Pt. However, Pd is a good dissociator of hydrogen; subsurface hydrogen reduces the availability for surface reactions, and the weaker adsorption of hydrogen on aromatic rings further hinders the hydrogenation rate[42]. However, a more balanced interaction between hydrogen and the aromatic substrates was observed for Pt, enabling it to perform better as a catalyst[43]. These findings indicate that Pt is significantly more active than

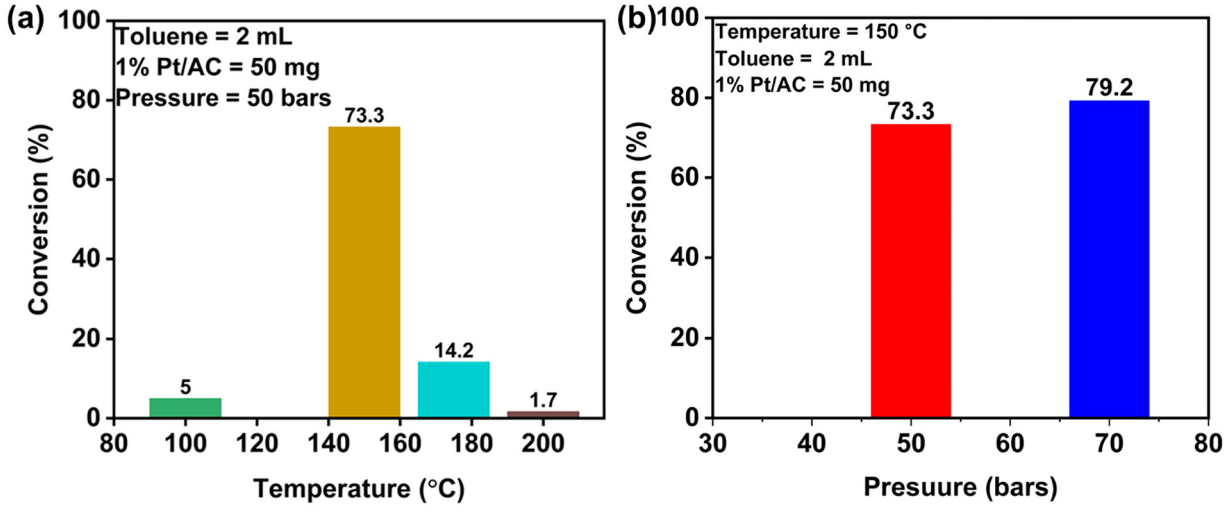


Figure 7. Effect of reaction conditions on toluene hydrogenation over 1 % Pt/AC catalyst: (a) Influence of temperature (100–200 °C) at 50 bar H2 and (b) influence of hydrogen pressure (50–70 bar) at 150 °C; reaction conditions: 2 mL toluene, 50 mg catalyst

Pd and that the addition of sulfur has a negative impact on the catalytic activity, which can probably be explained by changes in the metal–support interactions and potential site blocking. According to the results of the screening, 1% Pt/AC was the most efficient catalyst, and it was selected for parametric analysis.

Figure 7 shows how the performance of the selected 1% Pt/AC catalyst is affected by the temperature of the reaction and hydrogen pressure. Figure 7a demonstrates that temperature is a significant factor that defines the catalytic activity. The low conversion of 5% at 100 °C shows poor reaction kinetics. Increasing the temperature to 150 °C markedly increases the conversion to 73.3%, achieving optimum activation of hydrogen and improved reaction rates. Further heating to 175 and 200 °C, however, causes a drastic reduction to 14.2% and 1.7%, respectively. This decrease with temperature may be explained by the thermodynamic limitations of the exothermic hydrogenation reaction, possible deactivation of the catalysts, or decreased adsorption of reactants on the active sites. Figure 7b shows the effect of hydrogen pressure on the hydrogenation of toluene. An increment in pressure from 50 to 70 bar at 150 °C increases the toluene conversion from 73.3% to 79.2%. This result implies that an increase in the hydrogen partial pressure increases the availability of hydrogen on the surface, thus accelerating the kinetics of hydrogenation. However, the impact of pressure was not as significant as that of temperature. These findings suggest that reaction temperature is the most influential factor on catalytic performance, with an optimum at 150 °C, whereas an increase in hydrogen pressure offers a moderate improvement. The overall results of the catalyst screening and reaction parameter optimization suggest that 1% Pt/AC is the best system for toluene hydrogenation and holds significant potential for use in LOHC applications.

5. CONCLUSIONS

Pt- and Pd-based catalysts on AC and sulfur-doped carbon were prepared and tested for toluene hydrogenation as model LOHC systems. Structural and morphological studies proved that the catalysts mainly contained amorphous carbon frameworks with highly dispersed metal species, and sulfur doping had a strong impact on the support morphology and metal–support interactions. Catalytic analysis revealed that the catalytic activity was highly dependent on the type of active metal and support. The highest performance among the studied catalysts was achieved by 1% Pt/AC, which exhibited 73.3% conversion at 150 °C and 50 bar H_2. All catalysts had a high selectivity (>99%) to MCH. Pd-based catalysts and sulfur-doped systems were much less active, suggesting that the introduction of sulfur reduced the catalytic activity, probably because of site blocking or electronic effects. A parametric study of the 1% Pt/AC catalyst showed that reaction temperature was the most important parameter, and an optimum temperature of 150 °C was observed. Above this temperature, the conversion decreases, probably because of the thermodynamic constraints of the exothermic hydrogenation reaction. An augmentation of the hydrogen pressure stimulated the conversion rather modestly, which confirmed its secondary role in promoting catalytic activity. The results reveal that 1% Pt/AC is one of the most effective catalysts for hydrogenating toluene in LOHC systems.

AFFILIATIONS AND AUTHOR DETAILS

Undergraduate Author

Ghala Al Hetelah – *Materials Science and Engineering Department, King Fahd University of Petroleum & Minerals, Dhahran 31261, Saudi Arabia*; 0009-0007-7776-573X
Email: s202348430@kfupm.edu.sa

Corresponding Author

M. Nasiruzzaman Shaikh – *Lead Research Scientist, Interdisciplinary Research Center for Hydrogen Technologies and Carbon Management, King Fahd University of Petroleum & Minerals, Dhahran 31261, Saudi Arabia*; 0000-0002-9549-6322
Email: mnshaikh@kfupm.edu.sa

ACKNOWLEDGEMENTS

The authors acknowledge the support provided by the Department of Materials Science and Engineering (MSE) and the Interdisciplinary Research Center for Hydrogen Technologies and Carbon Management at the King Fahd University of Petroleum and Minerals. This research was funded by the Under-project No. INHT2521.

REFERENCES

(1) Hanley, E. S., Deane, J. P. & Gallachóir, B. P. Ó. The role of hydrogen in low carbon energy futures–A review of existing perspectives. *Renewable and Sustainable Energy Reviews* **82**, 3027–3045 (2018).

(2) Gómez, S. Y. & Hotza, D. Current developments in reversible solid oxide fuel cells. *Renewable and Sustainable Energy Reviews* **61**, 155–174 (2016).

(3) Tang, D. *et al.* State-of-the-art hydrogen generation techniques and storage methods: A critical review. *J. Energy Storage* **64**, 107196 (2023).

(4) dos Santos, K. G. *et al.* Hydrogen production in the electrolysis of water in Brazil, a review. *Renewable and Sustainable Energy Reviews* **68**, 563–571 (2017).

(5) Ali, A. & Shaikh, M. N. Recent developments in catalyst design for liquid organic hydrogen carriers: Bridging the gap to affordable hydrogen storage. *Int. J. Hydrogen Energy* **78**, 1–21 (2024).

(6) Rivard, E., Trudeau, M. & Zaghib, K. Hydrogen Storage for Mobility: A Review. *Materials 2019, Vol. 12, Page 1973* **12**, 1973 (2019).

(7) Zheng, J. *et al.* Development of high pressure gaseous hydrogen storage technologies. *Int. J. Hydrogen Energy* **37**, 1048–1057 (2012).

(8) Jorgensen, S. W. Hydrogen storage tanks for vehicles: Recent progress and current status. *Curr. Opin. Solid State Mater. Sci.* **15**, 39–43 (2011).

(9) Meng, J. *et al.* A Review of Catalysts for Methylcyclohexane Dehydrogenation. *Top. Catal.* **64**, 509–520 (2021).

(10) Atsumi, R. *et al.* Effects of steam on toluene hydrogenation over a Ni catalyst. *Appl. Catal. A Gen.* **590**, 117374 (2020).

(11) Yang, J. *et al.* Bimetallic Pd-M (M=Pt, Ni, Cu, Co) nanoparticles catalysts with strong electrostatic metal-support interaction for hydrogenation of toluene and benzene. *Molecular Catalysis* **492**, 110992 (2020).

(12) Zhao, S., Cai, J., Chen, H. & Shen, J. Understanding the effects of solvents on the hydrogenation of toluene over supported Pd and Ru catalysts. *Catal. Commun.* **157**, 106330 (2021).

(13) Han, W. *et al.* Coordinatively unsaturated aluminum anchored Ru cluster for catalytic hydrogenation of benzene. *J. Catal.* **400**, 255–264 (2021).

(14) Zhan, Y., Zhou, C., Jin, F., Chen, C. & Jiang, L. Ru/TiO2 catalyst for selective hydrogenation of benzene: Effect of surface hydroxyl groups and spillover hydrogen. *Appl. Surf. Sci.* **525**, 146627 (2020).

(15) He, H., Meyer, R. J., Rioux, R. M. & Janik, M. J. Catalyst Design for Selective Hydrogenation of Benzene to Cyclohexene through Density Functional Theory and Microkinetic Modeling. *ACS Catal.* **11**, 11831–11842 (2021).

(16) Guo, L., Xu, Z., Wang, T. & Zhu, H. Stable Pt/MgAl2O4 catalysts for efficient production of H2 from cyclohexane dehydrogenation. *Chem. Eng. Sci.* **299**, 120469 (2024).

(17) Fan, Y. *et al.* Continuous hydrogenation of N-ethylcarbazole in a micro-packed bed reactor for hydrogen storage. *Chemical Engineering Journal* **484**, 149404 (2024).

(18) Liu, H. *et al.* Ultralow Rh Bimetallic Catalysts with High Catalytic Activity for the Hydrogenation of N-Ethylcarbazole. *ACS Sustain. Chem. Eng.* **9**, 5260–5267 (2021).

(19) Zhao, X. *et al.* Ru-based catalysts for hydrogenation of N-ethylcarbazole: Progress and prospects. *Fuel* **360**, 130605 (2024).

(20) Li, J. *et al.* Dehydrogenation of dodecahydro-N-ethylcarbazole over spinel supporting catalyst in a continuous flow fixed bed reactor. *Fuel* **321**, 124034 (2022).

(21) Zhao, S. *et al.* A new insight into the kinetics of dibenzyltoluene hydrogenation over ruthenium catalyst for hydrogen storage. *Reaction Kinetics, Mechanisms and Catalysis* **137**, 1683–1699 (2024).

(22) Jeong, K. *et al.* Benzyl-methylbenzyl-benzene: Improving hydrogen storage and release performance of dibenzyltoluene based liquid organic hydrogen carrier. *Chemical Engineering Journal* **488**, 150927 (2024).

(23) Feng, X. *et al.* Boosting the hydrogenation activity of dibenzyltoluene catalyzed by Mg-based metal hydrides. *Int. J. Hydrogen Energy* **47**, 23994–24003 (2022).

(24) Liu, L. *et al.* Identifying Noble Metal Catalysts for the Hydrogenation and Dehydrogenation of Dibenzyltoluene: A Combined Theoretical-Experimental Study. *Inorg. Chem.* **62**, 17390–17400 (2023).

(25) Park, S., Abdullah, M. M., Seong, K. & Lee, S. Kinetic analysis of dibenzyltoluene hydrogenation on commercial Ru/Al2O3 catalyst for liquid organic hydrogen carrier. *Chemical Engineering Journal* **474**, 145743 (2023).

(26) Kerscher, M. *et al.* Thermophysical properties of the liquid organic hydrogen carrier system based on benzyltoluene considering influences of isomerism and dissolved hydrogen. *Int. J. Hydrogen Energy* **77**, 1009–1025 (2024).

(27) Dao, Q. N. *et al.* Catalytic insights into perhydro-benzyltoluene dehydrogenation: Probing surface characteristics revealed by DRIFTS study. *Int. J. Hydrogen Energy* **56**, 1284–1293 (2024).

(28) Bong, B. *et al.* Hydrogen Loading and Release Potential of the LOHC System Benzyltoluene/Perhydro Benzyltoluene over S–Pt/TiO2 Catalyst. *ACS Engineering Au* https://doi.org/10.1021/ACSENGINEERINGAU.4C00003 (2024) doi:10.1021/ACSENGINEERINGAU.4C00003.

(29) Li, J. *et al.* Intrinsic kinetics of benzyltoluene hydrogenation over a supported Ni catalyst for green hydrogen storage. *Int. J. Hydrogen Energy* **49**, 1586–1596 (2024).

(30) Park, H., Oh, J., Nguyen, T. B. & Lee, J. K. Hydrogen storage and release characteristics of polycyclic aromatic by-products for LOHC systems. *Appl. Catal. A Gen.* **636**, 118583 (2022).

(31) Niermann, M., Drünert, S., Kaltschmitt, M. & Bonhoff, K. Liquid organic hydrogen carriers (LOHCs) – techno-economic analysis of LOHCs in a defined process chain. *Energy Environ. Sci.* **12**, 290–307 (2019).

(32) Murata, K. *et al.* Enhancement of toluene hydrogenation activity of supported Pt nanoparticles with increasing the crystallinity of Pt. *Appl. Catal. A Gen.* **629**, 118425 (2022).

(33) Atsumi, R. *et al.* Kinetic Analysis of Support Effects of Pt-loaded Catalysts on Toluene Hydrogenation at Ambient Pressure. *Journal of the Japan Petroleum Institute* **62**, 28–36 (2019).

(34) Pushkarev, V. V., An, K., Alayoglu, S., Beaumont, S. K. & Somorjai, G. A. Hydrogenation of benzene and toluene over size controlled Pt/SBA-15 catalysts: Elucidation of the Pt particle size effect on reaction kinetics. *J. Catal.* **292**, 64–72 (2012).

(35) Lang, H., May, R. A., Iversen, B. L. & Chandler, B. D. Dendrimer-Encapsulated Nanoparticle Precursors to Supported Platinum Catalysts. *J. Am. Chem. Soc.* **125**, 14832–14836 (2003).

(36) Konuspayev, S., Shaimardan, M., Annas, N., Abildin, T. S. & Suleimenov, Y. Y. Hydrogenation of benzene and toluene over supported rhodium and rhodium-gold catalysts; Hydrogenation of benzene and toluene over supported rhodium and rhodium-gold catalysts. https://doi.org/10.1051/matecconf/202134001026 doi:10.1051/matecconf/202134001026.

(37) Zhao, S., Cai, J., Chen, H. & Shen, J. Understanding the effects of solvents on the hydrogenation of toluene over supported Pd and Ru catalysts. *Catal. Commun.* **157**, 106330 (2021).

(38) Yang, Y. *et al.* Supported mesoporous Pt catalysts with excellent performance for toluene hydrogenation under low reaction pressure. *Molecular Catalysis* **524**, 112341 (2022).

(39) Brandiele, R. *et al.* The interplay between surface area and sulfur doping of carbon support on Pt NPs nucleation and growth: A synergistic enhancement of catalytic activity for oxygen reduction. *Applied Catalysis B: Environment and Energy* **344**, 123620 (2024).

(40) Qiao, X. *et al.* Precious Metals Catalyze the Saturated Hydrogenation of Polycyclic Aromatic Hydrocarbons in Coal Tar. *Catalysts 2025, Vol. 15, Page 397* **15**, 397 (2025).

(41) Pal, M., Pal, P. & Nandi, M. Heteroatom-Doped Porous Carbons for Binder-Free and Metal-Free Supercapacitors: Design Strategies and Future Perspectives. *ChemNanoMat* **12**, e202500734 (2026).

(42) Bian, H., Kang, H., Zhong, W., Zhao, J. & Liang, T. Hydrogen diffusion into Pd(1 0 0) subsurface: Role of co-adsorbed bicomponent species on surface. *Appl. Surf. Sci.* **533**, 147448 (2020).

(43) Gonda, M., Ohshima, M. A., Kurokawa, H. & Miura, H. Toluene hydrogenation over Pd and Pt catalysts as a model hydrogen storage process using low grade hydrogen containing catalyst inhibitors. *Int. J. Hydrogen Energy* **39**, 16339–16346 (2014).